Stress wave radiation from brittle crack extension by molecular dynamics and FEM

P. Hora[a,*], O. Červená[a], A. Uhnáková[b], A. Machová[b], V. Pelikán[a]

[a]*Institute of Thermomechanics AS CR, v.v.i., Veleslavínova 11, 301 14 Plzeň, Czech Republic*
[b]*Institute of Thermomechanics AS CR, v.v.i., Dolejškova 5, 182 00 Praha, Czech Republic*

Abstract

We present results for molecular dynamic (MD) and finite element (FEM) simulations in 3D bcc iron crystals, with embedded central through crack (001)[110] of Griffith type, loaded in mode I. The sample geometry and border conditions in MD were chosen in such a way as to invoke a cleavage crack extension. Acoustic emission (AE) sources caused by the crack were analysed on both the atomistic and continuum level with FEM.
© 2013 University of West Bohemia. All rights reserved.

Keywords: molecular dynamics, finite element simulation, bcc iron crystal

1. Introduction

Crack (001)[110] (crack plane/crack front) can extend in a brittle manner, as atomistic simulations under plane strain conditions (e.g. [8]), but also fracture experiments on iron crystals [10, 11] have shown. However, behaviour at the crack front depends not only on the stress intensity K_I, but also on the so-called T-stress acting parallel to crack plane [2]. Change of the T-stress from negative to positive values may recall the ductile-brittle transition, as indicated in atomistic simulations under bi–axial loading, as well as continuum predictions [2]. The change of T-stress can also be recalled due to the geometry of a cracked sample under uni-axial tension, as follows from [4]. It was utilized in 3D atomistic MD simulations [14] together with special boundary conditions to invoke cleavage fracture. As mentioned in [14], AE sources from MD are well visible in the planes perpendicular to the crack front, but not in the crack plane due to a continuous bond breakage in the atomistic sample. It is a reason why surface Rayleigh waves cannot be recognised in the crack plane from MD.

In this paper we repeat 3D atomistic simulations from [14] where cleavage crack extensions have been invoked along the whole crack front. Here we treat somewhat shorter crack in comparison with [14]. Acoustic emission sources in 3D, recalled by the brittle fracture, are analysed on both the atomistic and FEM level utilizing new information from MD on residual forces in the crack plane during crack propagation.

2. MD and FEM simulations

Here we consider a pre-existing central crack of $2l_0 = 2a$ length, embedded in a rectangular sample. The crack surfaces lie on (001) planes, the crack front is oriented along the z-direction

---

*Corresponding author. Tel.: +420 377 279 652, e-mail: hora@cdm.it.cas.cz.

[110] and the potential crack extension is in the $x = [\bar{1}10]$ direction. The crack is loaded uni-axially in mode I, i.e. the sample borders are loaded in $y \langle 001 \rangle$ directions. Due to the symmetry of the problem, we simulate only one half of the sample in the x-direction. To maintain the symmetry, the atoms lying on the left border plane are fixed in the x-direction. The other atoms are free to move in the x-, y- and z-directions, excepting surface atoms on $\{110\}$ surfaces that are fixed in the z-direction. This serves to decrease stress concentration and prevent the plastic process at the corners, where the crack front penetrates the free surfaces. We utilize an N-body potential for bcc iron of Finnis-Sinclair type [1]. Interatomic interactions across initial crack faces are prevented, in order to simulate a pre-existing crack occurring in continuum models and in linear fracture elastic mechanics (LEFM).

The half crack length is $l_0 = 178 \, d_{110}$, where $d_{110} = a_0 \sqrt{2}/2$ and $a_0 = 2.8665 \, \text{Å}$ is the lattice parameter [1] and the initial half crack opening is $c_0 = d_{001}/2 = a_0/4$. The thickness of the crystal corresponds to 30 layers (110) in the z-direction parallel to the crack front. Crystal consists of 300 planes $[\bar{1}10]$ in the x-direction and 300 planes (001) in the y-direction. The total number of atoms in the atomistic sample is NPOIN= 1 350 000. The boundary corrections factors staying at stress intensity K_I [9] and at T-stress [4] correspond to $F_I \cong 3$ and to $G_I = +0.145$, where $G_I = \frac{T}{\sigma_A(1-\alpha)}$, $\alpha = l_0/W = 0.6$ and W is the half sample width.

Newtonian equations of motion for individual atoms are solved by a central difference method, using time integration step $h = 1 \times 10^{-14} \, \text{s}$. We use a ramp loading, i.e. the sample is loaded up to a level σ_A gradually (linearly) during 4000 time steps, as in [14]. When a prescribed stress level σ_A is reached, the applied stress is held constant.

Prior to external loading, the atomistic samples are relaxed to avoid the influence of surface relaxation on the microscopic processes at the crack front. Initial atomic velocities are set to zero and further atomic motion is not controlled in the system, similar to earlier work, e.g. in [14]. The global energy balance $W_{ext}(t) = E_{pot}(t,0) + E_{kin}(t)$ in the sample is monitored at each time step to check that the time step is sufficient to maintain energy conservation and numerical stability in the system. Here, $W_{ext}(t)$ denotes the work (calculated independently) done by the external forces distributed homogeneously in 6 upper and lower surface layers $\{001\}$, $E_{pot}(t,0) = E_{pot}(t) - E_{pot}(0)$ is the change of total potential energy during loading, and $E_{kin}(t)$ is total kinetic energy. The sum of interatomic interactions $LINT(t)$ in the system and the position of the crack front in the middle of the crystal are also monitored at each time step. At selected time steps, the local number of interactions (i.e. coordination number KNT), the local kinetic energies $E_{kin}(l_i)$ and the coordinates of individual atoms (l_i) are monitored for purposes of graphic treatment of the MD results. When bond breakage occurs in the atomistic system, residual atomic forces in the middle of the crack plane are monitored each time step for purposes of FEM. The basic elastic constants for the used potential are given in [1], the velocity of the longitudinal and transverse waves in the pure crystallographic directions $\langle 100 \rangle$, $\langle 110 \rangle$, $\langle 111 \rangle$ are given in [7], together with the matrix of elastic constants for our crystal orientation.

The wave motion modelling in the sample was carried out by using the finite element (FE) code COMSOL, [3]. The FE sample of width $150a_0\sqrt{2}$ and height $75a_0$ (quarter of the MD sample) was considered as a linear anisotropic elastic medium with cubic symmetry (3 inde-pendent elastic constants derived from the used potential in MD). Plane strain conditions inside the sample have been utilized in the anisotropic FE model of the same orientation as in MD. FE mesh consisted of 30000 quadrilateral elements with Lagrange Quadratic shape function. The element size was 0.2×0.2 nm. The problem was solved for 241 608 degrees of freedom. The FE sample is supposed to be without any initial stress/strain. For the time integration the full mass matrix and integration time step $\Delta t = 1 \times 10^{-14} \, \text{s}$ were used. The crack extension was
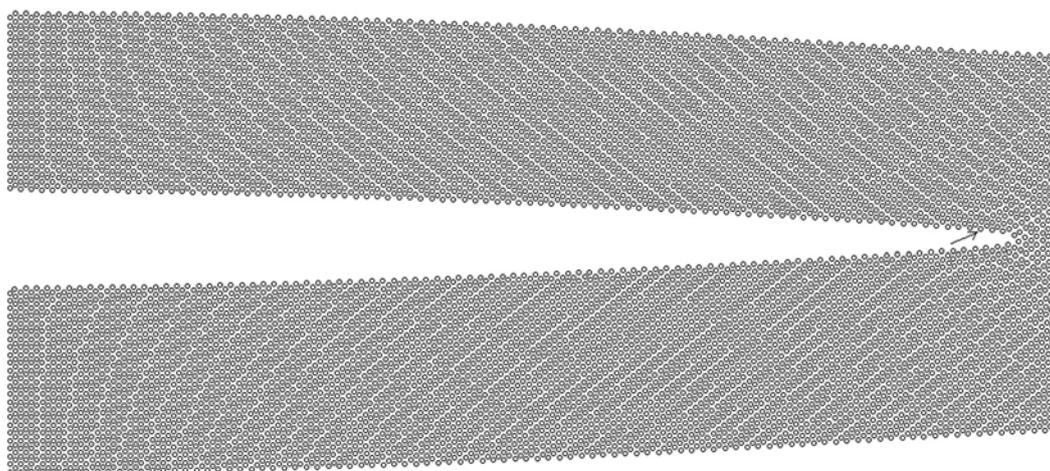
Fig. 1. New position of the crack front, at time step 4800 ($A = 0.897$ GPa), after crack initiation at time step 4614, detail in the middle of the 3D crystal

modeled by the prescribed residual forces in x and y directions at crack tip. These forces were obtained from MD simulation. This modelling of the crack extension is new and different from the approach used in [14], where the prescribed velocities were used.

3. Results and discussions

In MD, the applied constant stress level $\sigma_A = 0.897$ GPa was reached during 4000 time steps. Crack initiation in the middle of the crystal was monitored at time step 4614, at the applied critical Griffith stress intensity $K_A = F_I \sigma_A \sqrt{\pi l_0} = 0.911\,5$ MPa m$^{1/2}$ ($T = +0.052$ GPa). Fig. 1, at time step 4800, illustrates that crack initiation is brittle at both the sample surface and in the middle of the crystal. The initial position of the crack front is denoted in Fig. 1 by the arrow. Some incipient slip process is visible at the crack tip in Fig. 1a, but full development of twins (as in [12]) or dislocations (as in [13]) was not monitored, due to the used sample geometry and border conditions. The configuration is transient and disappears at free crack faces during crack advance; i.e. the fracture is brittle.

The half crack length at time step 4800 corresponds to $l = 184\,d_{110}$, i.e. the crack front is displaced by 6 interplanar distances in the bcc iron lattice in the $x = [\overline{1}10]$ direction. Each displacement of the crack front is accompanied by bond breakage and a stress relaxation at the crack front, which causes acoustic emission (AE) of the stress waves in the 3D crystal. This stress wave radiation can be monitored via mapping of local kinetic energies of the individual atoms, as illustrated in Fig. 2, for two layers (110) perpendicular to the crack front in the middle of the crystal at time step 4800. The kinetic energies are scaled as $\sqrt{E_{kin}(l_i)/10^{-22}}$. The darker the colour, the higher the kinetic energy in the system. Both quasi–longitudinal (qL) and quasi-transverse (qT) stress waves can be generated during bond breakage in 3D crystal. The 6 partial AE events may be well recognized at the crack surface and in the $\langle 111 \rangle$ direction below the lower crack face. The crack in MD extends with an average speed of $v_{cr} \approx 614$ m/s. Section of the ray (wave) surfaces in the (110) plane is shown in Fig. 3. However, the crack movement in this run was not uniform, see Table 1. Here the primary qL-wave front, after the crack initiation, already approaches the right free sample border. It represents a map of group velocities, derived from 3D non-convex map of phase velocities for the elastic constants of the used potential.
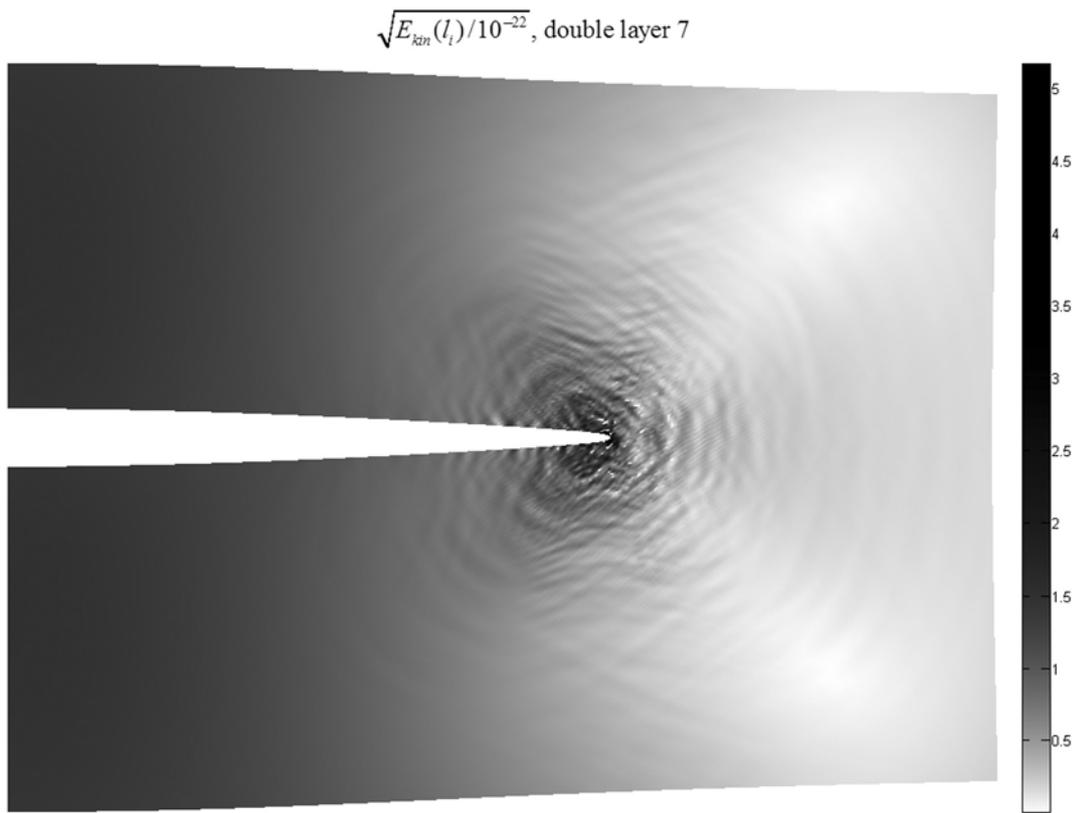
$\sqrt{E_{kin}(l_i)/10^{-22}}$, double layer 7

Fig. 2. Wave patterns from MD in the middle of the 3D crystal at time step 4800 on planes {110} perpendicular to the crack front
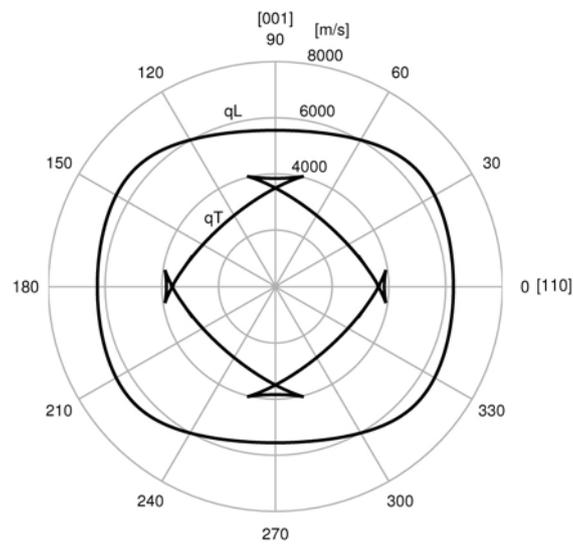

Fig. 3. Section of the ray (wave) surfaces in the (110) plane

Table 1. Dependence of the crack length on the time step

Time step	4614	4666	4779	4853	4944	5000
Crack length	$180\,d_{110}$	$182\,d_{110}$	$184\,d_{110}$	$186\,d_{110}$	$188\,d_{110}$	$190\,d_{110}$

Fig. 4. Time development of the new broken bonds (NBB) in the whole 3D crystal in MD

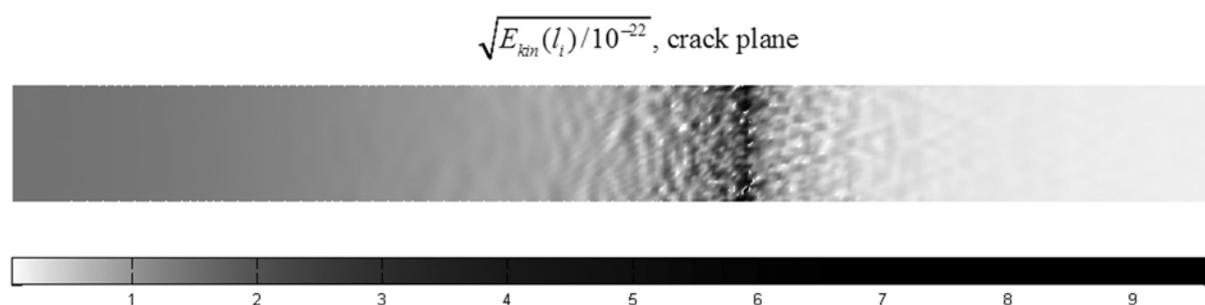$$\sqrt{E_{kin}(l_i)/10^{-22}} \text{, crack plane}$$

Fig. 5. Wave patterns from MD in the crack plane at time step 4800

The cross-lines coming from the qT-waves are visible in Fig. 2, mainly in the $\langle 001 \rangle$ directions, even below the wave fronts coming from the qL-waves. This can be explained by means of Fig. 4, where the number of broken bonds ($NBB = LINT(t)/2 - LINT(0)/2$) in the whole system is displayed and crack initiation is denoted by the letter i. It is clear that bond breakage in the system is a rather continuous process and thus the acoustic emission of the qT and qL-waves in the atomistic sample is also rather continuous, since each individual bond breakage acts as an AE-source. The qL-waves can be generated, e.g. by breaking of the second nearest neighbours in the bcc lattice, loaded in mode I. The qT-waves may be emitted after shear breaking of the bonds between the first nearest neighbours, since here the shear stress concentration in 3D is high. Note that generation of qT-waves during brittle fracture in 2D plane strain simulations [6, 7] was not discerned.

The first 2 bonds in the atomistic sample were already broken at time step 3776. After this first AE-event, the fastest longitudinal waves required approximately 388 time steps to reach the loaded borders in the $\langle 001 \rangle$ directions and the right free borders in the $\langle \overline{1}10 \rangle$ direction. The waves are reflected back into the crystal (back wave reflections) and they may already somewhat influence the situation at the crack front from time step 4552. Even before, the situation was influenced by back wave reflections in the z-direction, where the crystal is thin. The continuous bond breakage in Fig. 4 explains why some wave fronts, coming from the slower qT-waves, lie below the qL-wave fronts and also why the wave patterns in Fig. 5 in the crack plane are not well visible in MD. Moreover, scattering of loading stress waves at the crack front [7] and scattering of emitted stress waves on the discrete 3D atomic lattice, also complicate the recognition of wave patterns. Nevertheless, the strongest source of acoustic emission comes
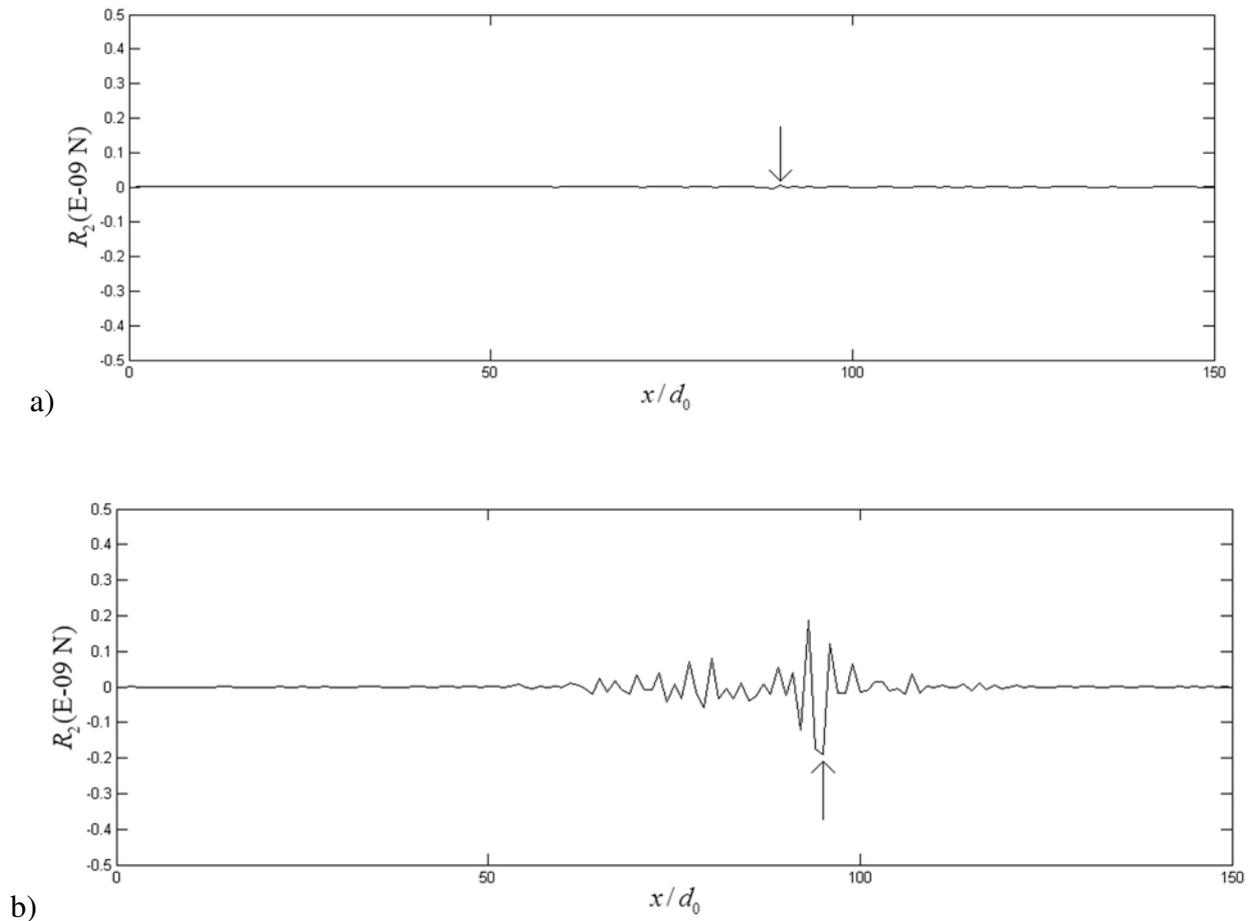
a)

b)

Fig. 6. Time development of the normal residual forces from MD in the crack plane, a) before the crack initiation at time step 3770, b) after the crack initiation at time step 5000. The crack front position is denoted by the arrow, $d_0 = a_0 \sqrt{2}$

from stress relaxation after crack initiation. The wave patterns in Fig. 2 are not influenced by the back wave reflections coming from this strongest AE source.

In comparison with dislocation emission [13] or twin generation [12], where qT-waves dominate in acoustic emission, cleavage crack extension in 3D invokes an AE source where qL-waves dominate, similar to 2D simulations in [6, 7] or continuum model in [5].

We also monitored time development of the residual forces in the middle of the crystal — see Fig. 6 where the crack front position before (Fig. 6a) and after crack initiation (Fig. 6b) is shown by the arrows. This information has been utilized in FEM simulations using the code [3].

The stress wave pattern obtained by elastic FEM simulations, of the dynamic process caused by crack tip hop, may be seen in Fig. 7. Plane strain conditions inside the sample were utilized in the anisotropic FEM model with the same orientation as in MD. All other boundary conditions correspond similarly to the MD case. The FE sample is supposed to be without any initial stress/strain.

Fig. 7 shows that, besides the qL-waves (at the sample borders) and qT-waves with the cross-lines (cusps), the wave source represented here by the residual forces, also generates Rayleigh waves (bright patterns behind the qT-waves) at the free crack surface (001). The surface Rayleigh waves are slower than qT-waves. They are polarized in $\{110\}$ planes and exist only close to the crack surface (001), as expected according to continuum analysis by
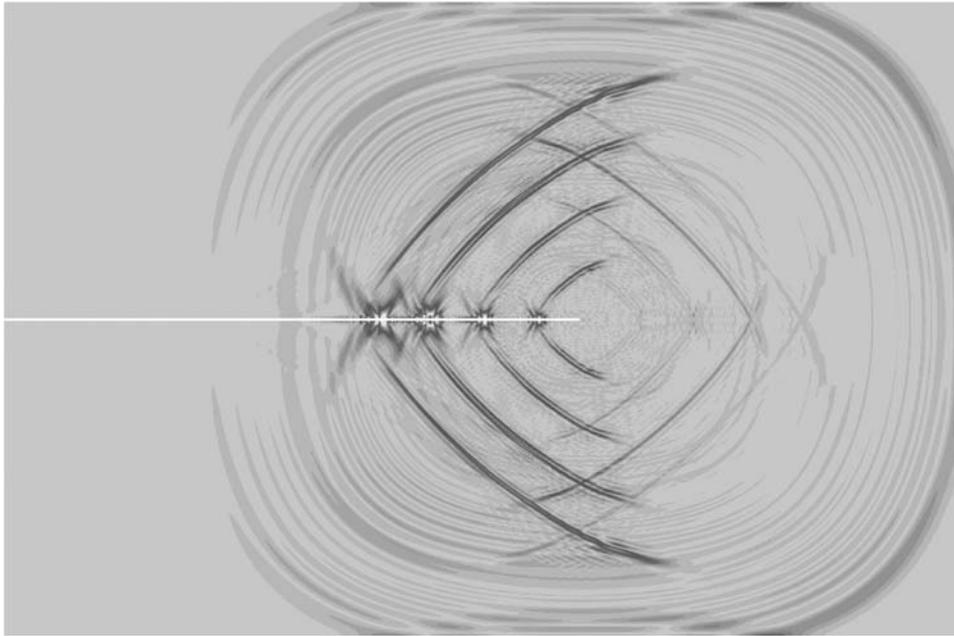
Fig. 7. Wave patterns from FEM modelling

Hearmon, presented e.g. in [7]. Due to the continuous bond breakage mentioned above and fast crack opening after crack initiation, the crack surface wave pattern is difficult to recognize from 3D atomistic simulations.

The results presented here and in [12, 13] are interesting for the experimental detection of acoustic emission by velocity sensitive transducers (see e.g. [6, 11]).

4. Summary

At higher applied loads, positive T-stress contributes to cleavage crack extension in MD. Under the ramp loading during 4000 time steps, the crack was initiated at the critical Griffith stress intensity.

MD simulations show that cleavage crack initiation in the 3D bcc iron crystal forms an AE-source, where qL-waves dominate. However, qT-waves are also generated during a continuous bond breakage in the crystal, which is new knowledge from 3D modelling. The strongest pulse emission comes from stress relaxation at the crack front, after the crack initiation.

Simplified modelling of the pulse emission by FEM shows that, besides the qL and qT–waves, Rayleigh waves can also be generated at the (001) free crack faces, in agreement with expectations according to continuum analysis.

Acknowledgements

References

[1] Ackland, G. J., Bacon, D. J., Calder, A. F., Harry, T., Computer simulation of point defect properties in dilute Fe–Cu alloy using a many-body interatomic potential, Philosophical Magazine A 75 (1997) 713–732.

[2] Beltz, G. E., Machová, A., Effect of T-stress on dislocation emission in iron, Scripta Materialia 50 (2004) 483–487.

[3] COMSOL, Inc., http://www.comsol.com.

[4] Fett, T., A compendium of T-stress solutions, Forschungszentrum Karlsruhe GmbH, 1998.

[5] Freund, L. B., Rosakis, A. J., The structure of the near tip field during transient elastodynamic crack growth (Research report), Brown University, Division of Engineering, R.I.02912, Providence, 1991.

[6] Landa, M., Machová, A., Převorovský, Z., Červ, J., Adámek, J., Crack growth in single crystals of alpha-iron (3 wt.% Si), Czechoslovak Journal of Physics 48 (1998) 1 589–1 606.

[7] Machová, A., Ackland, G. J., Dynamic overshoot in α-iron by atomistic simulations, Modelling and Simulation in Materials Science and Engineering 6 (1998) 521–542.

[8] Machová, A., Beltz, G. E., Chang, M., Atomistic simulation of stacking fault formation in bcc iron, Modelling and Simulation in Materials Science and Engineering 7 (1999) 949–974.

[9] Murakami, Y., Stress intensity factor handbook, Vol. 1, Pergamon Press, Oxford, 1987.

[10] Prahl, J., Machová, A., Landa, M., Haušild, P., Karlík, M., Spielmanová, A., Clavel, M., Haghi-Ashtiani, P., Fracture of Fe–3wt%Si single crystals, Materials Science and Engineering A 462 (2007) 178–182.

[11] Spielmannová, A., Landa, M., Machová, A., Haušild, P., Lejček, P., Influence of crack orientation on the ductile-brittle behavior in Fe–3wt%Si single crystals, Materials Characterization 58 (2007) 892–900.

[12] Spielmannová, A., Machová, A., Hora, P., Transonic twins in 3D bcc iron crystal, Computational Materials Science 48 (2010) 296–302.

[13] Spielmannová, A., Machová, A., Hora, P., Crack induced stress, dislocations and acoustic emission by 3-D atomistic simulations in bcc iron, Acta Materialia 57 (2009) 4 065–4 073.

[14] Uhnáková, A., Machová, A., Hora, P., Červ, J., Kroupa, T., Stress wave radiation from cleavage crack extension in 3D bcc iron crystals, Computational Materials Science 50 (2010) 678–685.